Journal of the Mechanics and Physics of Solids 120 (2018) 68–78

Contents lists available at ScienceDirect

Journal of the Mechanics and Physics of Solids

journal homepage: www.elsevier.com/locate/jmps

Stress fluctuation, crack renucleation and toughening in layered materials

C-J. Hsueh[a], L. Avellar[a], B. Bourdin[b], G. Ravichandran[a], K. Bhattacharya[a,*]

[a] Division of Engineering and Applied Science, California Institute of Technology, Pasadena, CA 91125, United States
[b] Department of Mathematics, Louisiana State University, Baton Rouge, LA 70803, United States

ARTICLE INFO

Article history:
Received 22 December 2017
Accepted 18 April 2018
Available online 23 April 2018

ABSTRACT

It has been established that contrast in the elastic properties can lead to enhancement of fracture toughness in heterogeneous materials. Focussing on layered materials as a model system, we show that this enhancement is a result of two distinct phenomena – first, fluctuations in stress leading to regions where the stress intensity at the crack is considerably smaller than that of the macroscopically applied value; and second, the lack of stress intensity when a crack is at a compliant to stiff interface thereby requiring renucleation. Using theoretical, computational and experimental methods, we study two geometries – a layered material and a layered material with a narrow channel – to separate the two phenomena. The stress fluctuation is present in both, but renucleation is present only in the layered medium. We provide quantitative estimates for the enhanced toughness.

1. Introduction

Heterogeneity is ubiquitous both in manufactured and natural materials. Indeed, all materials are heterogeneous at some length scale, ranging from atomistic (defects, dislocations) to microscopic (composites, concrete) to large-scale macroscopic (seismic fault zones) (Bazant, 1989; Ben-Zion and Sammis, 2003; Bower and Ortiz, 1991; Meyers et al., 2008). In multiphase materials, heterogeneities are characterized through the contrast in properties of the constituent phases including elastic moduli, fracture toughness, and yield stress. With the advent of additive manufacturing, it is becoming feasible to fabricate materials with desired and complex microstructures. When the scale of the heterogeneities is small compared to the application of interest, it is advantageous to define overall and effective properties. These are not simple averages of the constituents, and this motivates the study of the relation between effective properties, the constituent materials and their microstructure.

The overall effective elastic properties of composites and layered materials has received considerable attention, and systematic bounds have been established both in the linear and the nonlinear regimes (Milton, 2002). Our interest concerns the understanding of the effective toughness – resistance to fracture – of heterogeneous materials and this is less well understood. It is recognized that material heterogeneity contributes to macroscopic toughening. Extensive modeling and simulations have shed light on the mechanics of various phenomena that contribute to toughening (He and Hutchinson, 1989; Hutchinson and Suo, 1991). Consequently, both intrinsic and extrinsic toughening mechanisms have been identified and studied; still relatively little is known regarding the mechanistic contributions to overall toughening of heterogeneous

* Corresponding author.
E-mail address: bhatta@caltech.edu (K. Bhattacharya).

https://doi.org/10.1016/j.jmps.2018.04.011
0022-5096/

materials (Cook et al., 1964; Ritchie, 2011). For example, in brittle matrix composites, while matrix cracking and fiber pull-out are identified as the major mechanisms contributing to toughening, the overall toughness of such materials is not fully quantified in terms of the toughening mechanisms (Evans, 1990).

Layered materials with alternating layers of materials with differing properties are the simplest form of model heterogeneous materials. Engineered materials such as fiber-reinforced composites are the three-dimensional analogs of layered materials. Hossain et al. (2014) studied the fracture of layered solids using a phase field approach and have shown that there could be a substantial increase in toughness – well beyond that of the constituents – due to contrast in elastic moduli and fracture toughness of the constituents. They attributed the toughening of layered materials to stress fluctuations in the layers and the need to renucleate as the crach approaches from the compliant to the stiff layer. Wang and Xia (2017) performed systematic fracture experiments and cohesive zone simulations on a layered material manufactured through additive manufacturing. Their experiments showed that they could enhance toughness of the layered materials beyond those of the constituents.

In examining these detailed studies, two effects emerge as major contributors to overall toughening of heterogeneous composite materials: stress fluctuations and crack renucleation. For example, when a unidirectional fiber reinforced composite is loaded in tension along the fiber direction, there arise large stress fluctuations due to the mismatch in elastic properties between the fiber and matrix. In brittle matrix composites, initially, cracking occurs in the matrix between the fibers and don't propagate through the fibers. Due to the elevated stress in the fiber adjacent to the matrix crack, cracks renucleate in the matrix region adjacent to the stressed fibers (Evans, 1990). Such renucleation leads to further matrix cracking, which contributes to the overall toughening of the material. While these two mechanistic reasons for overall toughening has been known for the past few decades, there has been no systematic study of the effect of each of the mechanisms on toughening of heterogeneous materials.

The overall goal of the present study is to understand the effect and difference between the two effects: stress fluctuations and crack renucleation, and their contribution to the overall toughening of heterogenous materials. A related goal is to understand how the renucleation at the bimaterial interface (e.g., fiber-matrix interface) depends on the nature of the singularity. The two effects are explored systematically by studying a simple geometry, alternating layers of differing elastic moduli with and without a central channel. The former has both stress fluctuations and renucleation while the latter has only stress fluctuation. Further, the stress singularity at the interface between depends on the elastic contrast, which we relate to renucleation. Finally, we only consider situations where the interface is tough. If the interface is weak, then the cracks deflect into the interface as analyzed in detail by He and Hutchinson (1989).

A computational model using phase field fracture approach for designing and interpreting experiments is presented in Section 2. We use this model in Section 3 to study the layered microstructure with and without a stripe, and use it to study the contribution of stress fluctuation and renucleation to the overall toughness. We then turn to experimental studies, explaining the methods and material systems in Section 4. The measured fracture properties and observations of stress fluctuations and renucleation are discussed in Section 5. We conclude in Section 6 with a discussion.

2. Computational approach

We use the phase field fracture approach (Bourdin, 2007; Bourdin et al., 2000, 2008; Francfort and Marigo, 1998) for our simulations. This is a regularized method where we introduce a scalar field v taking values in [0,1] to describe the material states with regions with $v = 0$ representing intact material and regions with $v > 0$ representing regularized cracks. We have an energy functional

$$\mathcal{E}^{\ell}(u,v) = \int_{\Omega} \frac{(1-v)^2}{2} e(u) : C : e(u) + \frac{3G}{8}\left(\frac{v}{\ell} + \ell|\nabla v|^2\right) dx \tag{1}$$

where C is the elastic modulus, $e(u)$ is the strain associated with the displacement u, G is the critical energy release rate and ℓ is an internal length. It can be rigorously shown that this phase field fracture functional in Eq. (1) approximates (i.e., Γ-converges to) the classical brittle fracture functional when the internal length ℓ approaches 0 (Ambrosio and Tortorelli, 1990). We subject the body to some time-dependent boundary condition and at each time we minimize the energy subject to boundary condition and the constraints that v is monotone increasing and $0 \le v \le 1$. The solutions are characterized by crack-like regions of width $O(l)$ which are the regularized cracks. It has been shown that cracks nucleate in this model when the stress reaches a critical value that depends on the domain and the loading mode. In uniaxial tension, the critical stress is

$$\sigma_c = \sqrt{\frac{3GE}{8\ell}}. \tag{2}$$

Notice that this critical stress for crack nucleation increases with decreasing ℓ, and thus we may regard ℓ as a parameter that determines crack nucleation (Bourdin et al., 2014; Tanné et al., 2018). We refer the reader to Bourdin (2007) for details of the numerical implementation.

Following Hossain et al. (2014), we use the so-called surfing boundary condition for our simulations. This is a time-dependent steadily translating crack opening displacement field:

$$u^*(x_1, x_2, t) = U(x_1 - vt, x_2) \tag{3}$$

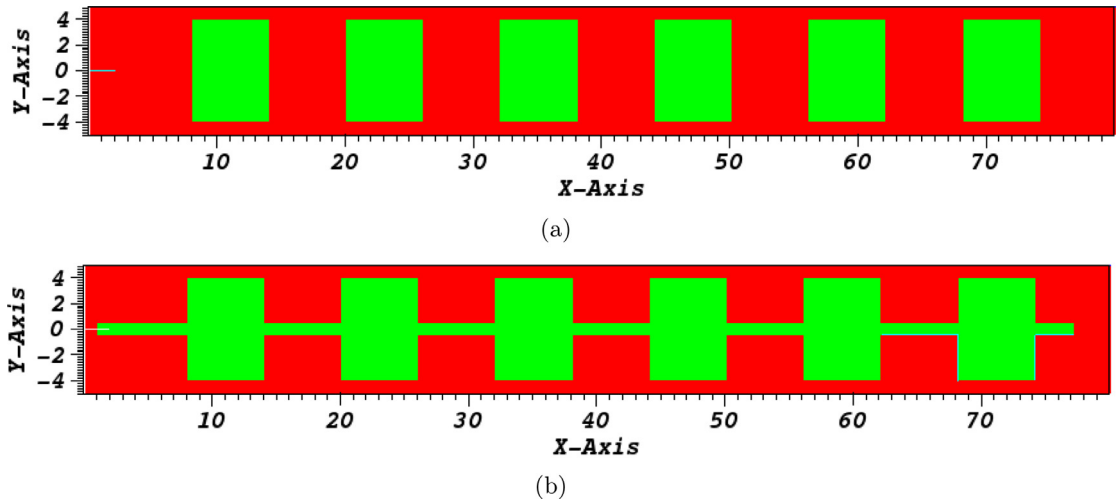

Fig. 1. (a) Layered microstructure with alternating layers of stiff (red online) and compliant (green online) materials. (b) Layered microstructure with a central channel or stripe. The stress heterogeneity is present in both, but the crack has to renucleate only in the layered medium. (For interpretation of the references to colour in this figure legend, the reader is referred to the web version of this article.)

with U to be the mode I crack opening field

$$U(x_1, x_2) = \frac{K_I}{2\mu}\sqrt{\frac{r}{2\pi}}(\kappa - \cos\theta)\left(\cos\frac{\theta}{2}\hat{e}_1 + \sin\frac{\theta}{2}\hat{e}_1\right). \tag{4}$$

for some fixed stress intensity factor K_I, effective shear modulus μ, effective bulk modulus κ, $r = \sqrt{x_1^2 + x_2^2}$, $\theta = \arctan(x_2/x_1)$ and v is the translation velocity. This boundary condition forces a macroscopic mode I crack opening that translates at a steady velocity, but does not in any way constrain the crack growth at the microscopic scale. In particular, if the material is heterogeneous, the crack can propagate in an unsteady manner, meander, branch, nucleate daughter cracks etc. As it does so, the forces on the boundary fluctuate. We compute the energy release rate or $J-$integral at the boundary at each instant; this fluctuates and we take the peak value to be the effective toughness. If the domain is large compared to the scale of the heterogeneities and if the crack(s) is(are) sufficiently far from the boundary, then the $J-$integral is path independent (Hsueh and Bhattacharya, 2016). Further, the effective toughness is independent of the specific form of U and of v (Hossain et al., 2014).

3. Computational results and theory

We study two microstructures shown in Fig. 1. All the results are presented in non-dimensional units. Fig. 1(a) shows a microstructure with alternating layers while Fig. 1(b) shows a microstructure with alternating layers with a thin central channel running through it. We assume a plane strain condition where both constituent materials have uniform toughness $G_c = 1$, Poisson's ratio $\nu = 0$ and internal length $\ell = 0.45$. However, the Young's moduli are different $E_s = 1$ in the stiff phase (red) material and either $E_c = 0.5$ or $E_c = 0.667$ in the compliant (green) material. The thin central channel is always made of the compliant material. We introduce a crack on the left and use the surfing boundary condition to drive the crack to the right. Given the symmetry of the microstructure and the loading, the crack remains straight. However, it propagates in an unsteady manner as the state of stress is not uniform. Further, it is forced to move from one material to another in the layered microstructure but is always confined to one material in the presence of the central channel. Heuristically, the stress distribution is similar in both materials, but one has renucleation in the layered material (Fig. 1(a)) but not in the layered material with a channel (Fig. 1(b)).

Fig. 2 shows the results of crack propagation in the layered material. Note from Fig. 2(a) that the crack is pinned at the interface going from the compliant to the stiff material leading to a rise in the $J-$integral. This determines the effective toughness and we note that this is significantly higher than the uniform material value of 1 thereby demonstrating the toughening by elastic heterogeneity. The effective toughness is shown for two separate contrasts and for various layer thickness in Fig. 2(b). We see that the effective toughness increases with contrast, and it increases with layer thickness reaching an asymptotic value for large layer thickness.

Fig. 3 shows the corresponding result of in the layered material with a central channel. We again see the toughening, but note that the amount of toughening is smaller in this case. These results for the two materials are contrasted in Fig. 4.

We now examine the mechanisms for the toughening. First, the state of stress is not uniform, and thus the crack-tip experiences different driving force. This stress heterogeneity mechanism is operative in both materials. Second, the driving

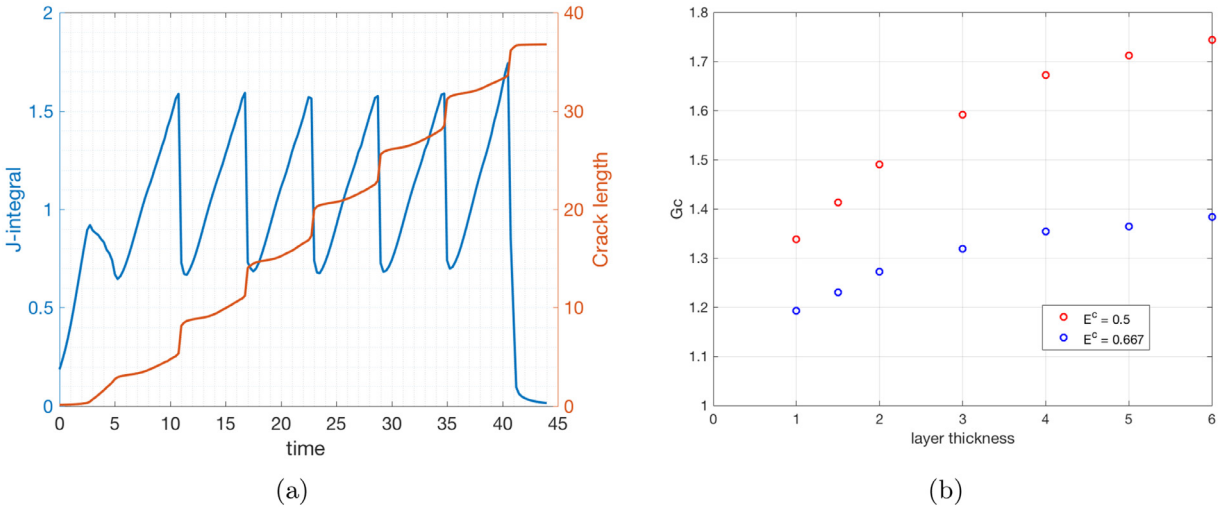

Fig. 2. Crack propagation through the layered material. (a) Crack-tip position and $J-$integral vs. time with $E^c = 0.5$ and layer thickness 4. (b) Effective toughness vs. layer thickness for two separate elastic contrasts. $E^s = 1$ for all calculations.

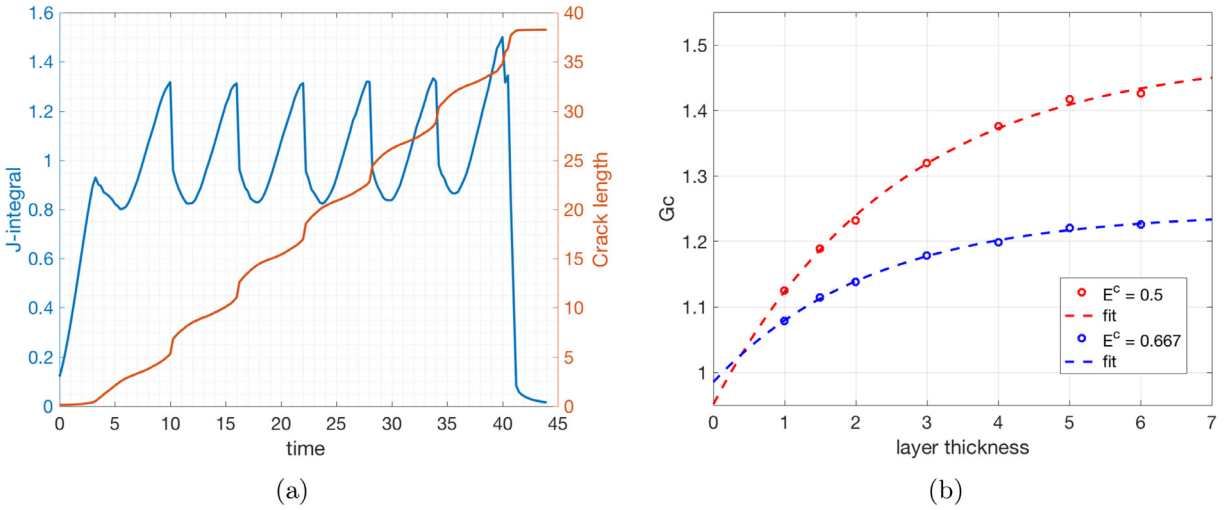

Fig. 3. Crack propagation through the layered material with a channel. (a) Crack-tip position and $J-$integral vs. time with $E^c = 0.5$ and layer thickness 4. (b) Effective toughness (G_c) vs. layer thickness (t) for two elastic contrasts. The dashed lines are the exponential fits $G_c^{eff} = c_0 + c_1 e^{-\frac{t}{c_2}}$. $E^s = 1$ for all calculations.

force on the crack decreases to zero as it approaches the compliant to stiff interface in the layered material, and thus the crack has to renucleate at the interface. This renucleation mechanism is operative only in the layered material.

We now propose a simple model to estimate the toughening due to stress heterogeneity. Consider a layered microstructure of two materials with Young's modulus $E^s > E^c$ subjected to a tensile load along the layers. Compatibility dictates that the longitudinal strain in both layers to be the same. This implies that the ratio between the stress in a material and the average stress is equal to the ratio of the Young's modulus of the material and to the average Young's modulus:

$$\varepsilon^s = \varepsilon^c \quad \Longrightarrow \quad E^{eff} = \langle E \rangle, \quad \frac{\sigma^i}{\langle \sigma \rangle} = \frac{E^i}{\langle E \rangle} \qquad i = s, c \tag{5}$$

where $\langle \cdot \rangle$ indicates the volume average. If the layer thickness is sufficiently large (specifically the K-dominant region is in a single layer) and the crack-tip is in material i, then the stress-intensity factor at the crack-tip is proportional to the stress σ^i in the material i. It follows from Irwin's formula $G = (1-\nu^2)\frac{K_I^2}{E}$ that the energy release rate

$$G^i = C\frac{|\sigma^i|^2}{E^i} = C\frac{\langle \sigma \rangle^2}{\langle E \rangle}\frac{E^i}{\langle E \rangle} = G^i_{macro}\frac{E^i}{\langle E \rangle} \quad \Longrightarrow \quad \frac{G^i}{G^i_{macro}} = \frac{E^i}{\langle E \rangle} \tag{6}$$

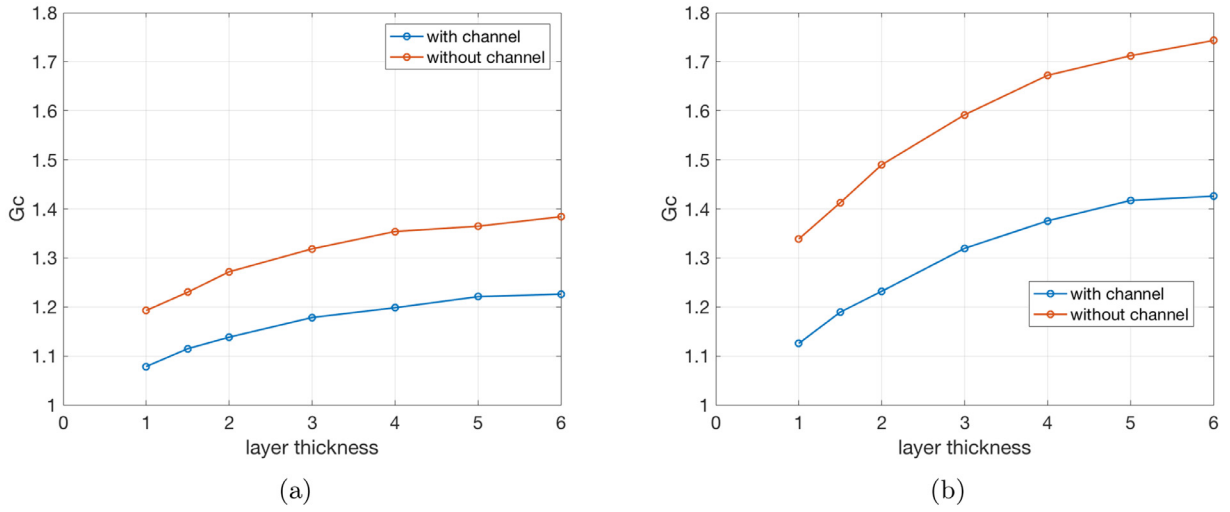

Fig. 4. Comparison of the toughening for the two microstructures for two separate elastic heterogeneities: (a) $E^c/E^s = 0.6674$ and (b) $E^c/E^s = 0.5$. Both microstructures result in toughening, but it is more pronounced in the case of the layered material (without the stripe/channel).

where C is a geometric factor and G^i_{macro} is the macroscopic energy release rate when the crack-tip is in the ith layer, and we have used (5). In other words the ratio between local and macroscopic energy release rate is equal to the ratio between the local and average elastic modulus. Since $G = G_c$ for the crack to propagate, it implies that

$$G^{macro} = \begin{cases} \frac{G^c_c \langle E \rangle}{E^c} & \text{crack-tip in compliant material} \\ \frac{G^s_c \langle E \rangle}{E^s} & \text{crack-tip in stiff material.} \end{cases} \tag{7}$$

Since the effective toughness is given by the maximum macroscopic energy release rate,

$$G^{eff,sf}_c = \max \left\{ G^c_c \frac{\langle E \rangle}{E^c}, G^s_c \frac{\langle E \rangle}{E^s} \right\} \tag{8}$$

where we have used 'sf' to remind ourselves that this is the toughening by stress fluctuations. If $G^c_c = G^s_s = G_c$, then

$$G^{eff,sf}_c = G_c \frac{\langle E \rangle}{E^c}. \tag{9}$$

This simple model predicts that for our layered material with a channel, the effective toughness would be 1.25 when $E^c = 0.667$ and 1.5 when $E^c = 0.5$ since the two materials have equal volume fraction. These agree very well with the asymptotic values of 1.244 and 1.485 obtained in the simulations. Further, this result also shows that the crack is arrested in the compliant material, also in agreement with the results of our simulations. This excellent agreement gives us confidence that the toughening mechanism in the layered material with a channel is stress heterogeneity.

We now turn to the second mechanism, crack renucleation, that is also active in the layered material (without the channel). We begin by recalling a result of Zak and Williams (1962) who studied the state of stress when one has a semi-infinite crack whose tip is at the bi-material interface as shown in Fig. 5(a). They showed that the state of stress is singular, $\sigma \sim r^{-(1-\lambda)}$ and the order of singularity depends on the contrast in elastic moduli. Specifically, λ is the smallest positive root of

$$A\lambda^2 + B + C\cos\lambda\pi = 0 \tag{10}$$

where

$$A = -4\alpha^2 + 4\alpha\beta, \quad B = 2\alpha^2 - 2\alpha\beta_2\alpha - \beta + 1, \quad C = -2\alpha^2 + 2\alpha\beta - 2\alpha + 2\beta \tag{11}$$

and

$$\alpha = \frac{k-1}{4(1-\sigma_1)}, \quad \beta = \frac{1-\sigma_1}{1-\sigma_2}k, \quad k = \frac{E_1(1+\nu_2)}{E_2(1+\nu_1)}, \quad \sigma_i = \frac{\nu_i}{1+\nu_i}. \tag{12}$$

We plot λ as a function of the ratio of the moduli (with $\nu_i = 0$ as in our simulations) in Fig. 5(b).

Note that when the crack goes from the compliant to the stiff material, $E_1/E_2 = E_c/E_s < 1$, then the order of singularity is less than half, and therefore the $J-$integral which determines the energy release rate or the driving force at the crack-tip is zero. In other words, the crack has to renucleate at this interface. On the other hand, when the crack goes from the stiff

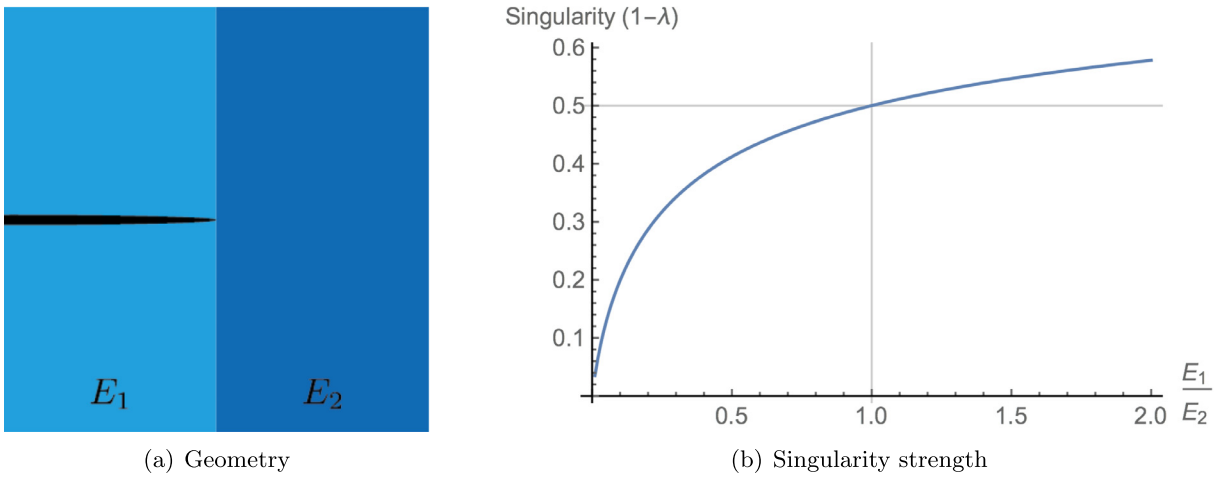

(a) Geometry (b) Singularity strength

Fig. 5. (a) Crack-tip at bi-material interface. (b) Order of the stress singularity at the crack-tip as a function of the elastic modulus contrast across the interface.

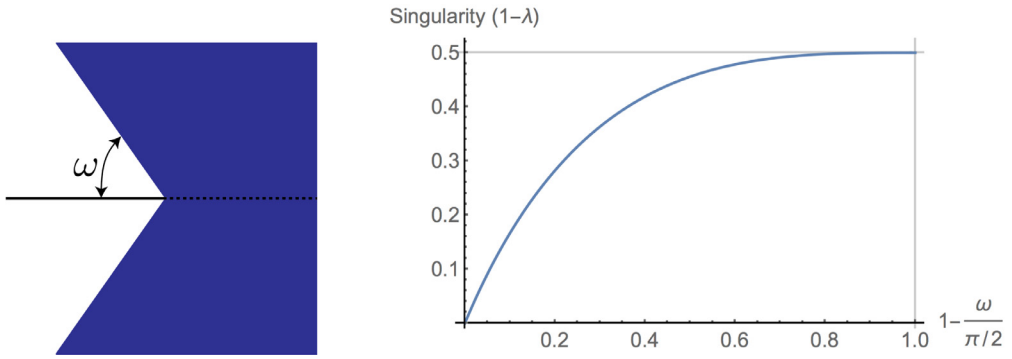

(a) Angle notch (b) Singularity

Fig. 6. An angle notch has weaker singularity.

to the compliant material, $E_1/E_2 = E_s/E_c > 1$ and the $J-$integral is infinite implying that the crack is likely to jump across this interface. Both of these are consistent with our computations.

Since the crack has to renucleate at this interface, one has to apply additional driving force which manifests itself as a higher effective toughness. This additional stiffness is the difference between the effective toughness of layers with and without a stripe (Fig. 4).

We now provide a quantitative estimate of this additional toughening by recalling the recent result of Tanné et al. (2018) who studied crack nucleation in a notched specimen shown in Fig. 6(a). The stress is again singular at the notch, $\sigma \sim r^{-(1-\lambda)}$ with λ the smallest positive root of

$$\sin(2\lambda(\pi-\omega)) + \lambda \sin(2(\pi-\omega)) \tag{13}$$

with ω half the opening angle of the notch. The stress singularity is shown in Fig. 6(b). Notice that we have the crack-tip singularity of half only when $\omega = 0$ or the notch closes into a crack. The order of the singularity is less than half, and consequently the $J-$integral is zero when $0 < \omega \leq \pi/2$. Tanné et al. (2018) proposed a crack nucleation criterion at the notch depending on the order of the singularity.

They define a generalized stress-intensity factor

$$K = \left.\frac{\sigma_{\theta\theta}}{r^{\lambda-1}}\right|_{r\to 0} \tag{14}$$

and say that the crack nucleates when this generalized stress-intensity factor reaches a critical value k_c that depends on λ. Their simulations are well approximated by

$$K_c = K_{Ic}^{2-2\lambda}\sigma_c^{2\lambda-1} \tag{15}$$

where K_{Ic} is the critical stress intensity factor and σ_c is the critical stress at which a crack nucleates at a free edge. Notice that when $\omega = 0$, $\lambda = 1/2$ and the criterion (15) reduces to the classical crack propagation criterion $K_I = K_{Ic}$, and when

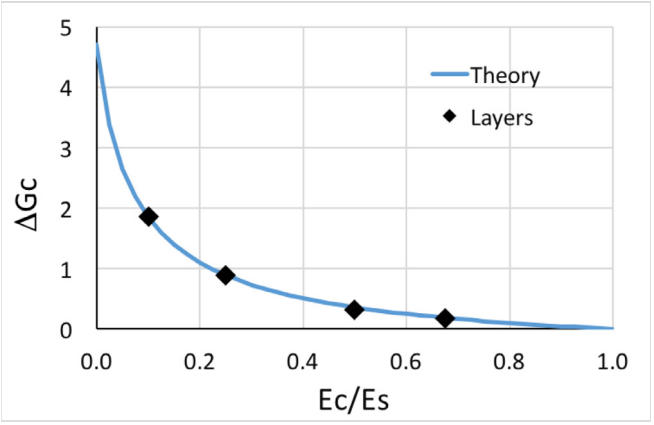

(a) Toughening due to renucleation

Fig. 7. Toughening due to renucleation.

Table 1
Nominal properties of the two constituent materials.

	E (MPa)	ν	G_c (kJ/m^2)	σ_u(MPa)
VeroWhite	1960	0.40	0.943	50
DM8530	1030	0.41	27.6	39

$\omega = \pi/2$, $\lambda = 1$ and the criterion (15) reduces to the classical critical stress crack nucleation criterion $\sigma = \sigma_c$. They also showed that their results are in agreement with numerous experimental observations.

We use this crack nucleation criterion (15) to study the excess toughening due to renucleation at the interfaces in our layered system. For our configuration, we define the generalized stress intensity factor as

$$K = \frac{\sigma}{L^{\lambda-1}} \tag{16}$$

where σ is the macroscopic stress and L is a configuration dependent characteristic length. The crack nucleates when $K = K_c$ or using (15)

$$\frac{\sigma_f}{L^{\lambda-1}} = K_{Ic}^{2-2\lambda}\sigma_c^{2\lambda-1} = \frac{K_{Ic}L^{\lambda-1}}{l_{ch}^{\frac{2\lambda-1}{2}}} \tag{17}$$

where σ_f is the stress at which failure occurs, and we have defined a material length $l_{ch} = (K_{Ic}/\sigma_c)^2$. We can use (2) to infer that $l_{ch} = 3/8l$ for our computational model. Now, the failure stress is related to the effective critical energy release rate

$$G_c^{eff,rn} = L\frac{\sigma_f^2}{E} \tag{18}$$

where we use 'rn' to indicated that this is toughening due to renucleation. Combining with (17) and using the fact that in plane strain $G_c = (1-\nu^2)K_{Ic}^2/E$, we obtain

$$G_c^{eff,rn} = \frac{G_c}{1-\nu^2}\left(\frac{L}{l_{ch}}\right)^{2\lambda-1}. \tag{19}$$

Fig. 7 compares this relation to the results of our computation for various moduli. We observe that we obtain an excellent agreement with $L = 0.962$. In particular, we see that the excess toughening of 0.178 and 0.317 for $E_c/E_s = 0.667$ and $E_c/E_s = 0.5$ agree very well with the difference in Fig. 4 between the toughness of a layered material with and without a stripe at large layer width. This excellent agreement gives us confidence that renucleation is necessary in the layered material, as well as in the relation between renucleation and stress singularity.

4. Experimental methods

We now examine the two mechanisms through experiments. We fabricate specimens with representative dimensions shown in Fig. 8 by printing them on a Stratasys Object500 Connex3 printer. We incorporate features such as holes, side groves and the initial crack during the printing, but create a sharp crack by pressing a razor blade into the printed crack. The printer uses proprietary materials: we chose VeroWhitePlus as our stiff material and DM8530 as our compliant material.

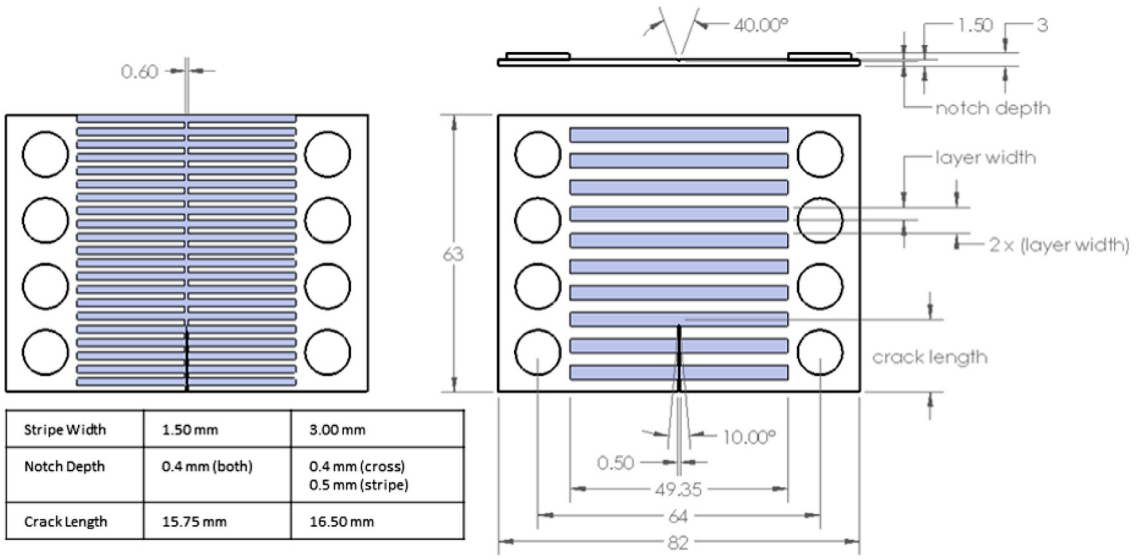

Stripe Width	1.50 mm	3.00 mm
Notch Depth	0.4 mm (both)	0.4 mm (cross) 0.5 mm (stripe)
Crack Length	15.75 mm	16.50 mm

Fig. 8. Representative specimen dimensions. Grey is DM8530; white is VeroWhite.

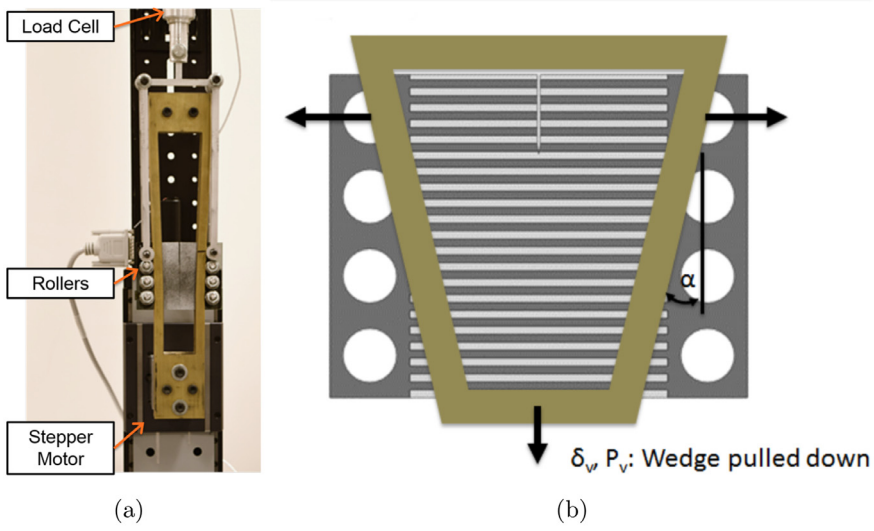

Fig. 9. (a) Picture of specimen in loading device including the brass rail. (b) Schematic of the specimen in the lodaing rail.

Their material properties are listed in Table 1.[1] Note that both materials and especially DM 8530 also undergo inelastic deformation. We will comment on this aspect later.

We alternate specimens of different types on the print bed in order to mitigate the effects of any local imperfections introduced by the printer. Additionally, the specimens are oriented at a 45° angle relative to the travel direction of the print head to ensure good interfacial bonding. Post-printing, specimens are stored in a sealed bag to mitigate exposure to air for five days prior to testing.

We load the specimens using the wedge setup shown in Fig. 9 to approximate the surfing boundary condition. Each loading hole in the specimen is fitted with a steel bushing and ball-bearing rollers. The rollers roll over a brass wedge with a smooth contact surface. The specimen is suspended from the top two loading holes, and the wedge is monotonically pulled down (with a PI M-410.CG motor controlled via a C-863 Mercury controller) at a rate of 0.5 mm per second. This causes an opening displacement δ between the two top holes of the specimen. The slope of the wedge ($\alpha = 2.2^\circ$) leads to an opening displacement 0.0383 mm per second. The load required for pulling is monitored (using an Interface Inc. WMC-25 load cell,

[1] The elastic moduli are obtained by uniaxial tensile tests, the critical energy release rate of VeroWhite by qualitative fractography, the critical energy release rate of DM8530 and ultimate strength from published values.

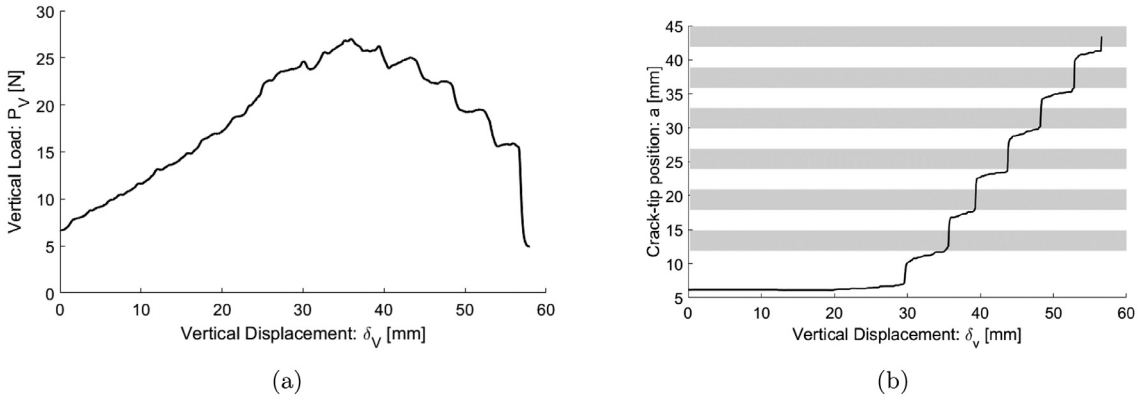

Fig. 10. Representative data. (a) Force vs. displacement and (b) Crack-tip position vs. displacement of the layered specimen S30001.

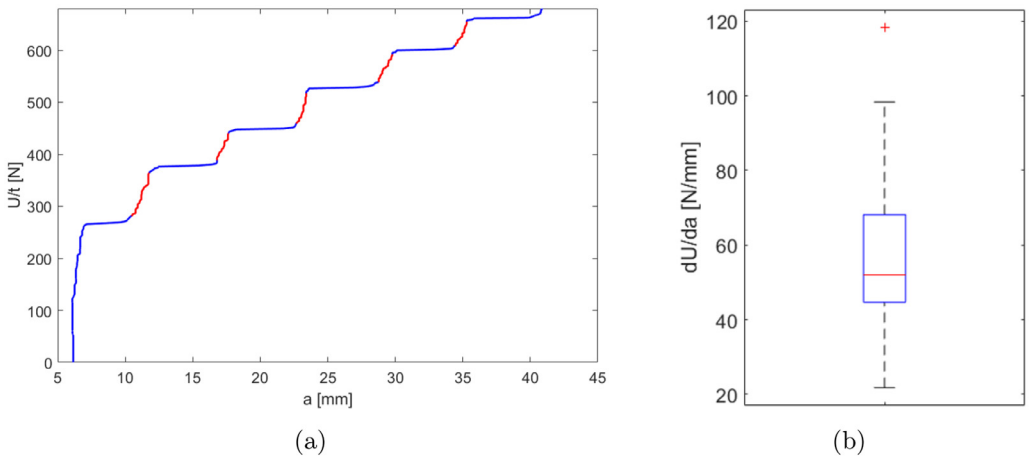

Fig. 11. (a) Representative results of integrating the horizontal load vs. horizontal displacement for specimen S30001 10–90% rise is highlighted (red online) b. Distribution of slopes for 3.0 mm layered specimens. Outliers are identified by crosses (red online). (For interpretation of the references to color in this figure legend, the reader is referred to the web version of this article.)

Omega DP25B-S-A1 strain meter and National Instrument USB-6251 BNC DAQ). The experiment is recorded with a Edmund Optics EO-1312M CCD Monochrome Camera. All data is acquired using a National Instrument LabView virtual instrument.

5. Experimental observations

Fig. 10(a) shows a representative force-displacement curves while Fig. 10(b) shows the position of the crack-tip as a function of the applied displacement for a layered specimen with layer width 3 mm. We see that the force increases roughly linearly till it reaches the peak. It then drops in a non-monotone fashion as the crack begins to grow in an unsteady manner. We also notice that the crack tip gets pinned at the interface between the stiff and compliant material, eventually breaks free and progresses slowly till it gets pinned again, and so forth. We observe a similar behavior in all specimens, layers with and without a channel and layer width 1.5 mm and 3 mm.

We use this data to extract the work done on the specimen as a function of the crack length. This is shown in Fig. 11(a). We obtain the work done on the specimen as a product of the measured load and applied displacement: $U = P_v\delta_v$. We see that U rises as the crack progresses slowly through the compliant region and remains steady as the crack jumps. For a steadily propagating crack, the energy release rate $G = \frac{\partial U}{\partial a}$. We are interested in the peak value since it describes the critical energy release rate necessary for the crack to propagate through this medium. To obtain this from our data, we look at the rising portion of the U vs. a curve and compute, $G = \frac{\Delta U}{\Delta a}$ using a linear regression of the points between the 90% and 10% values of the rising step (highlighted in Fig. 11(a)). We obtain a spread as shown in Fig. 11(b); we discard the outliers (generally associated with the first and last steps) and compute the average. The resulting values of the effective energy release rate is shown in Table 2.

We compare these with the predictions of the theory predicted in Section 3. We use (8) and the data in Table 1 to obtain the effective toughness of the layer with the channel as shown in Table 2. We see that the expected value of 40.1 kJ/m^2 for very wide layers agrees well with the experimentally observed value of 44.2 kJ/m^2 for 3mm layers. We use the renucleation

Table 2
Experimentally obtained values of G_c^{eff} in N/mm = kJ/m^2 for four specimens, along with the theoretically predicted values assuming large layer width.

Layer width [mm]	1.50	3.00	Theory
Layer with channel	28.8	44.2	40.1
Layer	31.2	56.2	57.5

criterion (15) or equivalently (19). We find l_{ch} from the ultimate strength of the material and L from the previous computational fit. We find that the anticipated valued of 57.5 kJ/m^2 agrees very well with the experimentally observed value of 56.2 kJ/m^2.

Together, this agreement gives us confidence in our understanding of the effect of stress fluctuation and renucleation on toughening in heterogeneous solids.

6. Discussion

In this paper, we have examined the pinning of cracks by elastic heterogeneities using theoretical, computational and experimental methods. It has been understood that elastic heterogeneities can lead to crack pinning due to two effects – the fact that the state of stress is heterogeneous and therefore the stress intensity at the crack tip may be smaller than the macroscopic value, and the fact that the stress intensity may vanish at the compliant to stiff interfaces and therefore the crack has to renucleate to penetrate the stiff material. We used two geometries – a layered material and a layered material with a narrow channel – to separate the two phenomena. The stress heterogeneity is present in both, but renucleation is present only in the layered medium.

We begin our discussion with the material with a compliant channel so that we only have the effect of stress heterogeneity. Our theoretical considerations show that under the assumption of uniform Poisson's ratio and very large layer width, the crack in the material with a channel would be pinned in the compliant material if $G_c^c \frac{\langle E \rangle}{E^c} > G_c^s \frac{\langle E \rangle}{E^s}$ and in the stiff material otherwise. This is confirmed through our computations. Since compliant materials typically have higher toughness, we expect the former to hold and the crack to always get pinned in the compliant material. This is indeed the situation in the material pair chosen for our experiments, and we observe that the crack gets pinned in the compliant layer in agreement with our prediction. Further, we expect from our computational results that the effective toughness increases with layer width and our experimental observations in Table 2 are in agreement. Finally, we see that the predicted value of effective toughness of 40.1 kJ/mm based on (8) agrees well with the experimentally observed value of 44.2 kJ/mm.

We now turn to the layered material without a compliant channel so that we have both the effect of stress heterogeneity and renucleation. As the crack approaches a compliant to stiff interface, the contrast in elastic modulus leads to a stress singularity that is less severe than the square-root of a crack-tip and consequently the stress-intensity factor falls to zero. Thus, the crack has to renucleate at the interface. We adopted the work of Tanné et al. (2018) to propose a criterion based on the notion of a generalized stress intensity factor that relates the excess toughening due to renuclueation to the order of the singularity to the renucleation. Our computations results are in very good agreement with this criterion. Our experimental results also show the effective toughness of a layered medium is higher in the absence of a channel confirming the toughening effect of renucleation. Indeed, our experimental value of 56.3 kJ/mm agrees well with the predicted value of 57.5 kJ/mm.

Our theoretical and computational analysis was limited to elastic materials while we did observe limited inelasticity in the experiments. The extension of this work to elastic plastic materials remains a topic for the future.

Author contributions

Hsueh and Avellar contributed equally to this work. Hsueh took the lead in developing the theoretical framework and the computational portion of the work. Avellar proposed the layers with and without stripe configuration and took the lead in the experimental portion of the work. All authors were involved in the conception of the project, analysis of the results and the drafting of the manuscript.

Acknowledgments

This work draws from the doctoral thesis of Chun-Jen Hsueh at the California Institute of Technology. We thank Suzanne Oliver for assisting with the determination of the properties of the homogeneous materials. We gratefully acknowledge the support of the US National Science Foundation through the Graduate Research Fellowship DGE-1144469 (Avellar) and Award no. DMS-1535083 and DMS-1535076 under the Designing Materials to Revolutionize and Engineer our Future (DMREF) Program (All authors).

References

Ambrosio, L., Tortorelli, V.M., 1990. Approximation of functional depending on jumps by elliptic functional via t-convergence. Commun. Pure Appl. Math. 43 (8), 999–1036.

Bazant, Z.P., 1989. Fracture energy of heterogeneous materials and similitude. In: Fracture of Concrete and Rock. Springer, pp. 229–241.

Ben-Zion, Y., Sammis, C.G., 2003. Characterization of fault zones. In: Seismic Motion, Lithospheric Structures, Earthquake and Volcanic Sources: The Keiiti Aki Volume. Springer, pp. 677–715.

Bourdin, B., 2007. Numerical implementation of a variational formulation of quasi-static brittle fracture. Interfaces Free Bound. 9, 411–430.

Bourdin, B., Francfort, G.A., Marigo, J.-J., 2000. Numerical experiments in revisited brittle fracture. J. Mech. Phys. Solids 48, 797–826.

Bourdin, B., Francfort, G.A., Marigo, J.-J., 2008. The variational approach to fracture. J. Elast. 91, 1–148.

Bourdin, B., Marigo, J.-J., Maurini, C., Sicsic, P., 2014. Morphogenesis and propagation of complex cracks induced by thermal shocks. Phys. Rev. Lett. 112, 014301.

Bower, A.F., Ortiz, M., 1991. A three-dimensional analysis of crack trapping and bridging by tough particles. J. Mech. Phys. Solids 39, 815–858. doi:10.1016/0022-5096(91)90026-K.

Cook, J., Gordon, J.E., Evans, C.C., Marsh, D.M., 1964. A mechanism for the control of crack propagation in all-brittle systems. Proc. R. Soc. Lond. A 282, 508–520.

Evans, A.G., 1990. Perspective on the development of high-toughness ceramics. J. Am. Ceram. Soc. 73 (2), 187–206. doi:10.1111/j.1151-2916.1990.tb06493.x.

Francfort, G.A., Marigo, J.-J., 1998. Revisiting brittle fracture as an energy minimization problem. J. Mech. Phys. Solids 46, 1319–1342.

He, M.-Y., Hutchinson, J.W., 1989. Crack deflection at an interface between dissimilar elastic materials. Int. J. Solids Struct. 25 (9), 1053–1067.

Hossain, M.Z., Hsueh, C.-J., Bourdin, B., Bhattacharya, K., 2014. Effective toughness of heterogeneous media. J. Mech. Phys. Solids 71, 15–32.

Hsueh, C.-J., Bhattacharya, K., 2016. Homogenization and path independence of the J-integral in heterogeneous materials. J. Appl. Mech. 83, 101012.

Hutchinson, J.W., Suo, Z., 1991. Mixed mode cracking in layered materials. Adv. Appl. Mech. 29, 63–191.

Meyers, M.E., Chen, P.-Y., Lin, A.Y-M., Seki, Y., 2008. Biological materials: structure and mechanical properties. Prog. Mater. Sci. 53, 1–206.

Milton, G.W., 2002. The Theory of Composites. Cambridge University Press.

Ritchie, R.O., 2011. The conflicts between strength and toughness. Nat. Mater. 10 (11), 817–822.

Tanné, E., Li, T., Bourdin, B., Marigo, J.J., Maurini, C., 2018. Crack nucleation in variational phase-field models of brittle fracture. J. Mech. Phys. Solids 110, 80–99.

Wang, N., Xia, S., 2017. Cohesive fracture of elastically heterogeneous materials: an integrative modeling and experimental study. J. Mech. Phys. Solids 98, 87–105. doi:10.1016/j.jmps.2016.09.004.

Zak, A.R., Williams, M., 1962. Crack Point Stress Singularities at a Bi-material Interface. Technical Report GALCIT-SM62-1. California Institute of Technology.